

Autonomous Underwater Vehicle Robust Path Tracking: Generalized Super-Twisting Algorithm and Block Backstepping Controllers

J. Guerrero*, J. Torres*, E. Antonio*, E. Campos**

**Department of Automatic Control, Center of Research and Advanced Studies of the National Polytechnic Institute (CINVESTAV), Mexico City, Mexico, (e-mail: {jguerrero,jtorres,eantonio}@ctrl.cinvestav.mx).*

*** CONACYT-Universidad del Istmo, Tehuantepec, Oaxaca, Mexico, (e-mail: ecampos@conacyt.mx)*

Abstract: This paper deals with the design and implementation of two nonlinear control strategies to solve the path-tracking problem for an Autonomous Underwater Vehicle (AUV) under model uncertainties and external disturbances. First, the AUV model is transformed into the so-called regular form by an appropriate selection of state variables. Afterward, the trajectory tracking problem is treated under two different perspectives; on the one hand, the Block Backstepping Control (BBSC) design was employed, in this methodology, the system into the regular form is rewritten regarding the error tracking dynamics and then the control law is obtained through a Lyapunov function stability analysis. The other method is based on the second order sliding mode technique known as Generalized Super-Twisting Algorithm (GSTA) which offers a way to ensure robustness to modeling errors and bounded external disturbances. Both control laws are designed to maintain a minimum margin of error in the trajectory tracking of the AUV even in the presence of damping and buoyancy disturbances. Finally, experimental results are also provided to illustrate the performances of the closed-loop system using proposed controllers.

Keywords: AUV, Sliding-mode control, Robust Control, Tracking Control, MIMO, Backstepping Control.

1. INTRODUCTION

Today, it has only been explored five percent of the ocean according to data from NOAA's Office of Ocean Exploration and Research. Within the field of maritime exploration, autonomous underwater vehicles (AUVs) have positioned themselves as an adequate choice for this kind of tasks because of remarkable benefits of its small scale.

In recent years, underwater vehicles have been widely used for the acquisition of physical variables of scientific interest in the deep sea, inspection of underwater structures, oceanographic mapping, maritime archaeology and so on. In general, the tasks mentioned require some level of autonomy of the vehicle, and that is why the interest in controlling the behavior of the underwater vehicle is so important. In this sense, there are three relevant control actions to provide autonomy to the vehicle: point stabilization, trajectory tracking, and path following control (Encarnacao and Pascoal, 2001).

Point stabilization refers to the problem of steering a vehicle to a final target point. Path following control aims at forcing a vehicle to converge to and follow a desired spatial path. Finally, Path tracking requires a vehicle to track a time-parameterized reference curve (Lapierre et al., 2003). In this work, we focus on the latter case, where the design of an AUV path-tracking controller is not a trivial task due to its

complex and highly nonlinear dynamics and unpredictable external perturbations such as the environmental force generated by the sea current fluctuation and the difficulty in accurately modelling the hydrodynamic effect. To control this type of vehicle have been proposed multiple control strategies: PD controllers (Hoang and Kreuzer, 2007), PID with nested saturations technique (Perrier and Canudas-De-Wit, 1996), Optimal Control (Wadoo et al., 2012), Neural Networks (Kawano and Ura, 2002; Szymak, 2016). Some of the applications listed use the linearized model of the vehicle, considering strong restrictive assumptions to simplify the mathematical description, resulting in an impractical controller due to its low robustness against disturbances (Akakaya et al., 2009; Wang et al., 2009). For this reason, many researchers concentrated their interests on the applications of robust control for underwater vehicles.

A broad class of controllers has been proposed for the path-tracking problem, for example, in (Li et al., 2015a) an adaptive fuzzy PID controller for tracking paths divided into line segments is used. A nonlinear PD scheme for both set-point regulation, as well as trajectory tracking for depth motion is proposed in (Campos et al., 2018). An adaptive tracking control capable of dealing with parametric uncertainties is shown in (Sahu and Subudhi, 2014). Moreover, in (Aguiar et al., 2007) a nonlinear Lyapunov-based tracking robust control law against parametric disturbances is shown. The Backstepping technique is used in

(Xiang et al., 2011) and a modified version of this methodology is shown in (Liang et al., 2016). Moreover, the use of the Backstepping control (BSC) is extended in work presented by (Li et al., 2015b), where a 3-D trajectory tracking control strategy of an AUV is considered. Linear stability is employed to obtain an output control loop for station keeping at some the desired velocity. Then, a Backstepping technique on the velocity error function is proposed. Computer simulation shows the trajectory tracking results, however, robustness against uncertainties on the damping and mass matrices is missing. Besides, in (Sun et al., 2014) a Bioinspired filtered Backstepping with Sliding Mode control for AUV trajectory tracking is developed. In this work, the AUV model of 4 degrees of freedom (x, y, z, yaw) is considered, the Backstepping methodology is used to control the AUV velocity in the body-fixed frame. Then, a component of the Bioinspired model is introduced into the BSC to avoid the sharp speed jumps due to large tracking errors which lead to increase the thrusters power consumption considerably. The added component works as a filter that will soften the sharp speed jump effect and produce smaller torques to avoid thruster's saturation. Afterward, the BSC law is used to design the sliding surface for Sliding Mode Control. In the designed controller, the signum function is replaced by an adaptive term to alleviate the chattering problem. Finally, simulation results show that the method of the filtered control minimizes the velocity error and, at the same time, the energy requirement in the thrusters is considerably reduced.

Sliding Modes is another robust control technique used in underwater vehicle control. High Order Sliding Mode Control (HOSMC) for position tracking, dynamic positioning or station keeping of an AUV device is considered in (Salgado-Jimenez et al., 2011). It is shown that exponential position tracking and velocity can be attained, with no acceleration measurements and avoiding chattering aftereffects. Advantages of HOSMC are evaluated concerning a conventional PID and a model-based first order sliding mode control through a simulation study. Finally, in (Ismail and Putranti, 2015) a second-order sliding mode controller namely, Super Twisting Algorithm (STA) is used to solve the AUV trajectory tracking problem in the (x - y) plane. In the cited paper, a robust controller is constructed in two parts, the nominal STA, and the equivalent control. In the development of the equivalent control, the concept of dynamic region is introduced, which consists of including a mathematical constraint in the form of a 2D region where the equivalent control action is confined and consequently low energy consumption by the vehicle is achieved. The results are presented only in simulation.

The main aim of this contribution is to present a comparative study between HOSMC and BSC as two of the most popular nonlinear robust control techniques used in trajectory tracking of UAVs. A sliding mode control of second order namely Generalized Super-Twisting Algorithm (GSTA) introduced by (Moreno, 2009) is adapted for trajectory tracking of an AUV and demonstrated its robustness under parameter uncertainties and external bounded disturbances through simulation and then validated by experimental results

for the first time. The GSTA methodology ensures robustness to modelling errors and external disturbances while reducing the chattering phenomenon caused by all first order sliding-mode based controllers. Moreover, the GSTA includes a linear version of the algorithm, the standard STA, and a STA with extra linear correction terms, that improves robustness and convergence velocity. In a second time, a Backstepping technique is considered. Contrary to other approaches, it is shown that working with the trajectory tracking error will allow reducing the Lyapunov stability analysis to two back steps only. As a consequence, the BSC law is easily obtained through a Lyapunov function analysis and the number of control gains is reduced to two parameters. Moreover, robustness against non-modelled dynamics (added mass and damping) is explicitly considered. Finally, the stability analysis of both control laws is proven by Lyapunov arguments. Besides the popularity of GSTA and backstepping as effective tools for robust control of non linear control one may emphasize the contribution of the present work as follows: 1) A systematic way to find the gains of the GSTA controller by solving a Linear Matrix Inequality (LMI) is given, 2) In order to have a complete robust stability analysis the perturbed case is considered which is very often case for the GSTA but not for the Backstepping algorithm, this issue was instrumental for being able to have a proper comparison between both control techniques, and 3) The performances and robustness have been evaluated in real time experiments.

The paper is organized as follows: In section II, the AUV model considered in this work is shown. Two control laws for trajectories tracking of the AUV based on the error are described in section III. In Section IV, an experimental evaluation of the performance of both controllers for trajectory tracking under damping and buoyancy disturbances is presented. Finally, in Section V conclusions and future work are presented.

2. DYNAMIC MODEL

The dynamic model of underwater vehicles has been described in several articles (see for instance (Fossen, 1994, 2002; Presterio, 2001; Kinsey et al., 2006)).

The dynamics of an underwater vehicle involves two frames of reference: the body-fixed frame and the earth-fixed frame (see Fig. 1). Considering the generalized inertial forces, the hydrodynamic effects, the gravity and buoyancy contributions as well as the forces of the actuators (i.e., thrusters), the dynamic model of an under water vehicle in matrix form, using the SNAME notation and the representation introduced by Fossen (1994), can be written as follows:

$$M\dot{v} + C(v)v + D(v)v + g(\eta) = \tau + \omega_e(t) \quad (1)$$

$$\dot{\eta} = J(\eta)v$$

Where $v = [u, v, w, p, q, r]^T$ is the state vector of velocity relative to the body-fixed frame and $\eta = [x, y, z, \phi, \theta, \psi]^T$ represents the vector of position and orientation relative to the earth-fixed frame. From equation (1), the matrix of spatial transformation between the inertial frame and the frame of the rigid body can be represented as $J(\eta) \in \mathbb{R}^{6 \times 6}$. $M \in \mathbb{R}^{6 \times 6}$ is the inertia matrix

where the effects of mass are included, $C(v) \in \mathbb{R}^{6 \times 6}$ is the Coriolis-centripetal matrix, $D(v) \in \mathbb{R}^{6 \times 6}$ represents the hydrodynamic damping matrix, $g(\eta) \in \mathbb{R}^6$ is the vector of gravitational/buoyancy forces and moments. Finally, $\tau \in \mathbb{R}^6$ is the control vector acting on the underwater vehicle and $\omega_e(t) \in \mathbb{R}^6$ defines the vector of external disturbances.

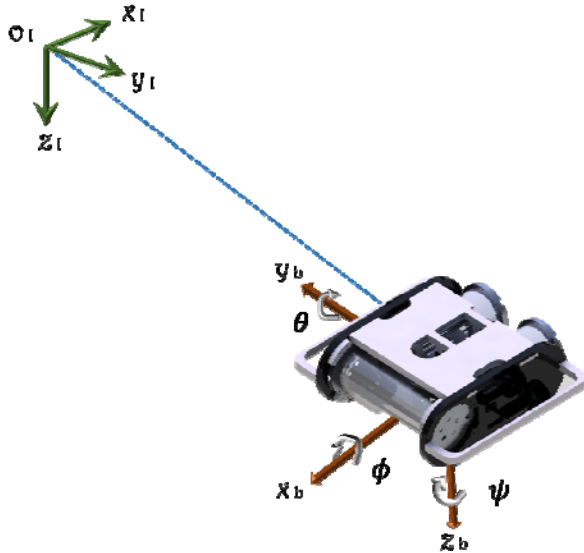


Fig. 1. An underwater vehicle with the inertial-fixed frame (O_I, x_I, y_I, z_I) and the body-fixed frame (O_b, x_b, y_b, z_b).

The presented formulation of the AUV dynamics is expressed in the body-fixed frame and can be transformed to the earth-fixed frame by using the kinematic transformations of the state variables and the model parameters as follows:

$$M_\eta(\eta) = J^{-T}(\eta) M J^{-1}(\eta)$$

$$C_\eta(v, \eta) = J^{-T}(\eta) [C(v) - M J^{-1}(\eta) \dot{J}(\eta)] J^{-1}(\eta)$$

$$D_\eta(v, \eta) = J^{-T}(\eta) D(v) J^{-1}(\eta)$$

$$g_\eta(\eta) = J^{-T}(\eta) g(\eta)$$

$$\tau_\eta = J^{-T}(\eta) \tau$$

The system (1) can, therefore, be represented in the earth-fixed frame as:

$$M_\eta(\eta) \dot{\eta} + C_\eta(v, \eta) \dot{\eta} + D_\eta(v, \eta) \dot{\eta} + g_\eta(\eta) = \tau_\eta(\eta) + \omega_\eta(t) \quad (2)$$

Hydrodynamic loads dominate the AUV dynamics, and it is difficult to accurately measure or estimate the hydrodynamic coefficients that are valid for all vehicle operating conditions. As such, the system dynamics are not exactly known. Therefore, the system dynamics $f(\eta, v)$ given in (2) can be written as the sum of estimated dynamics $\hat{f}(\eta, v)$ and the unknown dynamics $\tilde{f}(\eta, v)$ as follows:

$$f(\eta, v) = \hat{f}(\eta, v) + \tilde{f}(\eta, v) \quad (3)$$

Where:

$$\hat{f}(\eta, v) = \hat{M}_\eta(\eta) \dot{\eta} + \hat{C}_\eta(v, \eta) \dot{\eta} + \hat{D}_\eta(v, \eta) \dot{\eta} + \hat{g}_\eta(\eta) \quad (4)$$

$$\tilde{f}(\eta, v) = \tilde{M}_\eta(\eta) \dot{\eta} + \tilde{C}_\eta(v, \eta) \dot{\eta} + \tilde{D}_\eta(v, \eta) \dot{\eta} + \tilde{g}_\eta(\eta) \quad (5)$$

Moreover, the matrices of the unknown dynamics vector $\tilde{f}(\eta, v)$ are defined as $\tilde{M}_\eta = M_\eta - \hat{M}_\eta$, $\tilde{C}_\eta = C_\eta - \hat{C}_\eta$, $\tilde{D}_\eta = D_\eta - \hat{D}_\eta$, and $\tilde{g}_\eta = g_\eta - \hat{g}_\eta$.

Rewriting the system (2) into the estimated and unknown dynamics given by (3), we have:

$$\hat{M}_\eta(\eta) \dot{\eta} + \hat{C}_\eta(v, \eta) \dot{\eta} + \hat{D}_\eta(v, \eta) \dot{\eta} + \hat{g}_\eta(\eta) = \tau_\eta(\eta) + \omega(t) \quad (6)$$

where $\omega(t) = \omega_\eta(t) - \tilde{f}(\eta, v)$.

3. CONTROLLER DESIGN

In this section, the design of two types of controllers for the AUV is addressed. The first section describes the methodology to implement a controller based on the GSTA. The second section describes the procedure to construct the Block Backstepping Control law. Both are based on the trajectory tracking error.

3.1 Controller based on GSTA

The Super-Twisting algorithm is derived from the theory of sliding mode control. The main advantage of the Super-Twisting algorithm is its insensitivity to disturbance, in other words, the behaviour of the nominal design and disturbed, is the same. Due to the high frequency of the signum function used under this theory, an undesirable phenomenon known as chattering occurs. Where the introduction of the Super-Twisting algorithm, described as a sliding mode controller of the second order, reduce the impact of this phenomenon considerably. For the application of Super-Twisting controller, it is required to propose a sliding surface σ with relative degree one and minimum phase (Shtessel et al., 2014).

From (6) we introduce the next state variables:

$$x_1 = \eta$$

$$x_2 = \dot{\eta}$$

Rewriting the model as follows:

$$\dot{x}_1 = x_2$$

$$\dot{x}_2 = F(x) + G(x)u + \omega(t) \quad (7)$$

Where:

$$F(x) = -\hat{M}_\eta(\eta)^{-1} [\hat{C}_\eta(v, \eta) \dot{\eta} + \hat{D}_\eta(v, \eta) \dot{\eta} + \hat{g}_\eta(\eta)]$$

$$G(x) = \hat{M}_\eta(\eta)^{-1} J^{-T}(\eta)$$

$$u = \tau_\eta(\eta)$$

At this point, it is possible to describe a control law to force the state x_1 to follow the desired trajectory $x_1^d(t) = [x_d(t), y_d(t), z_d(t), \phi_d(t), \theta_d(t), \psi_d(t)]^T$ using the technique of inverse dynamics control. Now, it is necessary to make the following assumptions:

Assumption 1. The first and second derivatives of the desired trajectories are bounded.

Assumption 2. The perturbation $\omega(t)$ is a Lipschitz continuous signal.

Assumption 3. The roll, pitch, and yaw angles are limited to $(-\frac{\pi}{2} < \phi < \frac{\pi}{2})$, $(-\frac{\pi}{2} < \theta < \frac{\pi}{2})$ and $(-\pi < \psi < \pi)$.

According to assumptions 1 and 2, the external disturbance terms $\omega(t)$ are bounded

$$\|\omega_i(t)\|_2 \leq \delta_i, \quad i = \overline{1,6}. \quad (8)$$

also, satisfy the following inequality:

$$\|\dot{\omega}_i(t)\|_2 \leq L_i, \quad i = \overline{1,6}.$$

According to assumption 3, the matrix $G(x)$ is not singular, therefore, its inverse exists.

The Super Twisting controller acts on the dynamics of the error. From (7) it is possible to propose a sliding surface depending on the error that forces the sliding mode in the manifold as follows:

$$\sigma = \dot{e} + \Lambda \cdot e \quad (9)$$

where $e = x_1^d - x_1$, $\dot{e} = x_2^d - x_2 = \dot{x}_1^d - \dot{x}_1$

and $\Lambda = \text{diag}(\lambda_1, \lambda_2, \lambda_3, \lambda_4, \lambda_5, \lambda_6) \in \mathbb{R}^{6 \times 6}$ is a diagonal positive definite matrix.

Remark 1: The proposed sliding surface σ is a minimum phase and has relative degree one.

The proposed control law is shown below:

$$u = J^T M_{\eta}(\eta) [\ddot{x}_1^d + \Lambda \dot{e} - F(x) - v_{\text{GSTA}}] \quad (10)$$

Where the Super-Twisting controller, v_{GSTA} , is defined as follows:

$$\begin{aligned} v_{\text{GSTA}} &= -K_1 \phi_1(\sigma) + \lambda + \varphi \\ \dot{\varphi} &= -K_2 \phi_2(\tau) \end{aligned} \quad (11)$$

With:

$$\phi_1(\sigma) = |\sigma|^{\frac{1}{2}} \text{sgn}(\sigma) + \sigma \quad (12)$$

$$\phi_2(\sigma) = \frac{1}{2} \text{sgn}(\sigma) + \frac{3}{2} |\sigma|^{\frac{1}{2}} \text{sgn}(\sigma) + \sigma \quad (13)$$

The gains matrices $K_1 = \text{diag}(k_{11}, k_{12}, k_{13}, k_{14}, k_{15}, k_{16})$ and $K_2 = \text{diag}(k_{21}, k_{22}, k_{23}, k_{24}, k_{25}, k_{26})$ are definite positive.

3.1.1 Stability Analysis

In order to formalize the analysis of AUV robust path tracking based on sliding mode control theory let us give the following.

Theorem 1. Consider the system (6) and the Generalized Super-Twisting Algorithm with perturbation terms (11) in closed loop error dynamics given by (14). Suppose that the perturbation terms of the system (16) are globally bounded by some positive constants $\delta_1, \dots, \delta_6$. Then the gains K_1 and K_2 can be selected high enough so that the origin is an equilibrium point that is strongly globally asymptotically

stable, and all trajectories converge in finite time to the origin.

Proof. From (9) and (10), the closed loop dynamics is given by:

$$\dot{\sigma} = -K_1 \phi_1(\sigma) - K_2 \int_0^t \phi_2(\sigma(\tau)) d\tau + \omega(t) \quad (14)$$

Let:

$$\begin{aligned} s_{1i} &= \sigma_i \\ s_{2i} &= -k_{2i} \int_0^t \phi_2(\sigma_i(\tau)) d\tau + \omega_i(t) \\ \dot{\omega}_i(t) &= \beta_i(t) \end{aligned}$$

Then (14) can be rewritten in scalar form ($i = \overline{1,6}$) as:

$$\begin{aligned} \dot{s}_{1i} &= -k_{1i} \left[|s_{1i}|^{\frac{1}{2}} \text{sgn}(s_{1i}) + s_{1i} \right] + s_{2i} \\ \dot{s}_{2i} &= -k_{2i} \left[\frac{1}{2} \text{sgn}(s_{1i}) + \frac{3}{2} |s_{1i}|^{\frac{1}{2}} \text{sgn}(s_{1i}) + s_{1i} \right] + \beta_i(t) \end{aligned}$$

Without loss of generality, we can represent the system with simplified notation:

$$\dot{s}_1 = -k_1 \left[|s_1|^{\frac{1}{2}} \text{sgn}(s_1) + s_1 \right] + s_2 \quad (15)$$

$$\dot{s}_2 = -k_2 \left[\frac{1}{2} \text{sgn}(s_1) + \frac{3}{2} |s_1|^{\frac{1}{2}} \text{sgn}(s_1) + s_1 \right] + \beta(t)$$

Noting that $\phi_2(s_1) = \phi_1'(s_1) \phi_1(s_1)$ and selecting the vector $\chi = [\phi_1(s_1), s_2]$ and $\rho = \frac{\beta(t)}{\phi_1'(s_1)}$, it is possible to rewrite the system (1) as follows:

$$\dot{\chi} = \phi_1'(s_1) [A\chi + B\rho] \quad (16)$$

where the matrices are defined as follows:

$$A = \begin{bmatrix} -k_1 & 1 \\ -k_2 & 0 \end{bmatrix}, \quad B = \begin{bmatrix} 0 \\ 1 \end{bmatrix} \quad (17)$$

Case I. Unperturbed system: Consider the unperturbed system (1), choosing the Lyapunov candidate function (CLF) as follows:

$$V = \chi^T P \chi \quad (18)$$

where P is a positive definite matrix which satisfies the Lyapunov equation:

$$A^T P + P A = -Q \quad (19)$$

where Q is any given positive definite matrix and let λ_{\min} denote the smallest eigenvalue of Q .

Note that the proposed Lyapunov candidate function is a continuous, positive definite and differentiable function which satisfies the next form:

$$\lambda_{\min}(P) \|\chi\|_2^2 \leq V(s) \leq \lambda_{\max}(P) \|\chi\|_2^2 \quad (20)$$

Where $\|\chi\|_2^2 = |s_1| + 2|s_1|^2 + s_1^3 + s_2^2$ is the Euclidean norm of χ and noting that:

$$|\phi(s_1)| \leq \|\chi\|_2 \geq \frac{V^2(\chi)}{\lambda_{\min}^2(P)}$$

The time derivative of V along the trajectories of the system is:

$$\begin{aligned} \dot{V}(X) &= 2\chi^T P \dot{\chi} \\ &= \phi'_1(s_1) \chi^T (A^T P + PA) \chi \\ &= -\phi'_1(s_1) \chi^T Q \chi \\ &\leq -\phi'_1(s_1) \lambda_m \|\chi\|_2^2 \\ &\leq -\left[1 + \frac{1}{2|s_1|^2}\right] \lambda_m \|\chi\|_2^2 \\ &\leq -\lambda_m \|\chi\|_2^2 - \frac{\lambda_m}{2} \frac{\|\chi\|_2^2}{|s_1|^2} \\ &\leq -\alpha_1 V - \frac{\alpha_2}{2} \sqrt{V} \end{aligned}$$

where

$$\alpha_1 = \frac{\lambda_m}{\lambda_{\max}(P)}; \quad \alpha_2 = \frac{\lambda_m \lambda_{\min}^{\frac{1}{2}}(P)}{\lambda_{\max}(P)}$$

Note that V is continuously decreasing function and we can conclude that the equilibrium point is reached both exponentially and in finite time.

Since the solution of its analog differential equation:

$$\dot{v} = -\alpha_1 v - \alpha_2 v^{\frac{1}{2}}, \quad v(0) \geq 0 \quad (21)$$

is given by:

$$v(t) = \exp(-\alpha_1 t) \left[v(0)^{\frac{1}{2}} + \frac{\alpha_2}{\alpha_1} \left[1 - \exp\left(\frac{\alpha_1}{2} t\right) \right] \right]^2 \quad (22)$$

Moreover, using the comparison principle, the solution converges exponentially and in finite time to the origin as stated before. Finally, $s_i = 0$ in finite time and according to (9), this implies that $\lim_{t \rightarrow \infty} e = 0$ and $\lim_{t \rightarrow \infty} \dot{e} = 0$.

Remark 2: Note that the system (16) in the absence of disturbances, the necessary and sufficient condition for convergence is that the matrix A be Hurwitz. This equates to the condition $k_1 > 0$ and $k_2 > 0$.

Case II. Perturbed system: Consider the perturbed system (16) with the Lyapunov candidate function defined as (18). It is assumed that the transformed perturbation satisfy the sector condition (Moreno, 2009), it means:

$$\omega(\rho, \chi) = -\rho^2(\rho, \chi) + \rho(t, \chi) (L_{21}^T + L_{21}^T) \chi - \chi^T L_{22}^T L_{21}^T \chi \geq 0 \quad (23)$$

and considering that the upper and lower bounds of the perturbation are symmetric, it can be chosen as $L_{21}^T = -L_{22}^T = LC$ where $C = [1 \ 0]$. Then, we have:

$$\omega(\rho, \chi) = -\rho^2(\rho, \chi) + \chi^T L_{22}^T L_{21}^T \chi \quad (24)$$

$$= -\rho^2(\rho, \chi) + L^2 \chi^T C^T C \chi \geq 0 \quad (25)$$

To design purposes, it is important to note that the gain matrix A can be rewritten as:

$$A = A_0 - K_0 C_0 \quad (26)$$

where

$$A_0 = \begin{bmatrix} 0 & 1 \\ 0 & 0 \end{bmatrix}, \quad K_0 = \begin{bmatrix} k_1 \\ k_2 \end{bmatrix}, \quad C_0 = [1 \ 0] \quad (27)$$

The time derivative of V along the trajectories of the system is defined as follows:

$$\begin{aligned} \dot{V}(X) &= 2\chi^T P \dot{\chi} \\ &= \phi'_1(s_1) [\chi^T (A^T P + PA) \chi + \chi^T P B \rho + \rho^T B^T \chi] \\ &= -\phi'_1(s_1) \begin{bmatrix} \chi \\ \rho \end{bmatrix}^T \begin{bmatrix} A^T P + PA & P B \\ B^T P & 0 \end{bmatrix} \begin{bmatrix} \chi \\ \rho \end{bmatrix} \\ &\leq -\phi'_1(s_1) \left\{ \begin{bmatrix} \chi \\ \rho \end{bmatrix}^T \begin{bmatrix} A^T P + PA & P B \\ B^T P & 0 \end{bmatrix} \begin{bmatrix} \chi \\ \rho \end{bmatrix} + \omega(\rho, \chi) \right\} \\ &= -\phi'_1(s_1) \left\{ \begin{bmatrix} \chi \\ \rho \end{bmatrix}^T \begin{bmatrix} A^T P + PA + L^2 C^T C & P B \\ B^T P & -1 \end{bmatrix} \begin{bmatrix} \chi \\ \rho \end{bmatrix} \right\} \\ &= -\phi'_1(s_1) \left\{ \begin{bmatrix} \chi \\ \rho \end{bmatrix}^T \begin{bmatrix} A^T P + PA + L^2 C^T C + \bar{\alpha} P & P B \\ B^T P & -1 \end{bmatrix} \begin{bmatrix} \chi \\ \rho \end{bmatrix} \right\} \\ &\quad - \phi'_1(s_1) \bar{\alpha} \chi^T P \chi \\ &= -\phi'_1(s_1) \left\{ \begin{bmatrix} \chi \\ \rho \end{bmatrix}^T W(K_0, P | \bar{\alpha}, L) \begin{bmatrix} \chi \\ \rho \end{bmatrix} - \bar{\alpha} \chi^T P \chi \right\} \end{aligned}$$

where:

$$W(K_0, P | \bar{\alpha}, L) = \begin{bmatrix} W_{11} & W_{12} \\ W_{21} & W_{22} \end{bmatrix}$$

with:

$$W_{11} = A_0^T P + P A_0 + L^2 C^T C - C_0^T K_0^T P - P K_0 C_0 + \bar{\alpha} P$$

$$W_{12} = P B$$

$$W_{21} = B^T P$$

$$W_{22} = -1$$

Assuming that K_0 is selected in such way that exists $P > 0$ and $\bar{\alpha} > 0$ providing $W(K_0, P | \bar{\alpha}, L) \leq 0$. The time derivative of V can be expressed as follows:

$$\dot{V}(X) \leq -\bar{\alpha} \phi'_1(s_1) \chi^T P \chi \quad (28)$$

$$= -\frac{\bar{\alpha}}{2|s_1|^2} V - \bar{\alpha} V \quad (29)$$

$$\leq -\frac{\bar{\alpha}\lambda_{\min}^{\frac{1}{2}}(P)}{2}V^{\frac{1}{2}-\bar{\alpha}}V \quad (30)$$

The time derivative of V definite negative condition is reached by selecting the positive gains k_1 and k_2 high enough in order to satisfy the condition $W(K_0, P|\bar{\alpha}, L) \leq 0$. Therefore V converges to zero and following the same arguments stated in the unperturbed case, $s_i=0$ in finite time and according to (9), this implies that $\lim_{t \rightarrow \infty} e=0$ and $\lim_{t \rightarrow \infty} \dot{e}=0$.

Remark 3: The matrix $W(K_0, P|\bar{\alpha}, L) < 0$ is a Bilinear Matrix Inequality due to the product of P and K_0 . In order to solve this problem as a Linear Matrix Inequality (LMI) it can be introduced the following matrix:

$$Y = PK_0 \quad (31)$$

The matrix W can be rewritten in the next form:

$$W = \begin{bmatrix} -C_0^T Y^T - Y C_0 + \bar{\alpha} P & PB \\ A_0^T P + P A_0 + L^2 C^T C & \\ B^T P & -1 \end{bmatrix} \quad (32)$$

This representation of W can be seen as LMI on P and Y . Note that it is needed to know the bound of the disturbance and a fixed positive constant value $\bar{\alpha} > 0$ in order to solve the LMI (32) and be able to find the gains of the GSTA controller through the following relationship:

$$K_0 = P^{-1} Y \quad (33)$$

3.2 Backstepping Controller

The Backstepping controller design technique for robust path tracking has received a lot of contributions (see for instance Encarnacao and Pascoal (2001); Lapierre et al.(2003); Wang et al. (2009); Xiang et al. (2011); Liang et al.(2016); Aguiar and Hespanha (2007); Wu and Karkoub(2014))). For completeness, let us give an adapted version of it by the following.

Corollary 1. Consider the system (6) transformed into (7). Let $e_1 = x_1^d - x_1$ and $e_2 = x_2 - \dot{x}_1^d - \Gamma e_1$ the tracking errors and the gain diagonal positive definite matrices $\Gamma = \text{diag}(\gamma_1, \gamma_2, \gamma_3, \gamma_4, \gamma_5, \gamma_6) \in \mathbb{R}^{6 \times 6}$ and $Y = \text{diag}(v_1, v_2, v_3, v_4, v_5, v_6) \in \mathbb{R}^{6 \times 6}$.

If Assumptions A1-A3 are satisfied and proposing the following backstepping controller:

$$u = G(x)^{-1} [\ddot{x}_1^d + e_1 - F(x) - \Gamma(e_2 + \Gamma e_1) - Y e_2] \quad (34)$$

Then, the tracking errors e_1 and e_2 converge to zero asymptotically, with $V(e_1, e_2) = \frac{1}{2} e_1^T e_1 + \frac{1}{2} e_2^T e_2$ as a Lyapunov function.

Moreover, the norm of the error $\|e\|$ has an ultimately bounded performance when the system (7) under perturbations is considered and then the practical stability is proved.

Proof. Consider the undisturbed dynamic model shown in (7), i.e., $\omega(t)=0$, defining the tracking errors as:

$$\begin{aligned} e_1 &= x_1^d - x_1 \\ \dot{e}_1 &= \dot{x}_1^d - \dot{x}_2 \end{aligned} \quad (35)$$

We define the Lyapunov candidate functions as follows:

$$V_1(e_1) = \frac{1}{2} e_1^T e_1 \quad (36)$$

Differentiating the function (36) with respect to time and substituting (35):

$$\dot{V}_1(e_1) = e_1^T \dot{e}_1 = e_1^T (\dot{x}_1^d - \dot{x}_2) \quad (37)$$

Taking x_2 as the virtual control x_2^v and choosing:

$$x_2^v = \dot{x}_1^d + \Gamma e_1 \quad (38)$$

Substituting in (37), we have:

$$\dot{V}_1(e_1) = -e_1^T \Gamma e_1 \quad (39)$$

Choosing $\Gamma = \Gamma^T > 0$ this ensures the first state stabilization. Then, for stabilizing the second state, we need to define an error between the virtual control and the second state as follows:

$$e_2 = x_2 - x_2^v \quad (40)$$

Rewriting the system depending on the errors, we obtain:

$$\begin{aligned} \dot{e}_1 &= -\Gamma e_1 - e_2 \\ \dot{e}_2 &= \Gamma(\Gamma e_1 + e_2) - \ddot{x}_1^d + F(x) + G(x)u \end{aligned} \quad (41)$$

The following CLF is proposed:

$$V_2(e_1, e_2) = V_1(e_1) + \frac{1}{2} e_2^T e_2 \quad (42)$$

The derivative of the function (42) over time along the trajectories of the system (41) is given by:

$$\dot{V}_2 = -e_1^T \Gamma e_1 - e_2^T e_2 + e_2^T [F(x) + G(x)u + \Gamma(\Gamma e_1 + e_2) - \ddot{x}_1^d] \quad (43)$$

Now, introducing the control law (34) into (43) it follows that:

$$\dot{V}_2 = -e_1^T \Gamma e_1 - e_2^T Y e_2 \quad (44)$$

There is a suitable choice of gain matrices Γ and Y that makes (44) a negative definite function. Using standard Lyapunov arguments, the tracking errors e_1 and e_2 converge to zero asymptotically.

Perturbed case. The injection of the control law (34) into the error system (41) considering external disturbances, leads to the following closed-loop system:

$$\begin{aligned} \dot{e}_1 &= -\Gamma e_1 - e_2 \\ \dot{e}_2 &= e_1 - Y e_2 + \omega(t) \end{aligned} \quad (45)$$

The closed-loop system (45) can be represented as

$$\frac{d}{dt} \begin{bmatrix} e_1 \\ e_2 \end{bmatrix} = \begin{bmatrix} -\Gamma & -I_{6 \times 6} \\ I_{6 \times 6} & -Y \end{bmatrix} \begin{bmatrix} e_1 \\ e_2 \end{bmatrix} + \begin{bmatrix} 0 \\ 1 \end{bmatrix} \omega(t) \quad (46)$$

The error dynamics (46) can be expressed in compact form as

$$\dot{e} = Ae + B\rho \quad (47)$$

Where $e = [e_1, e_2]^T$ and $\rho = \omega(t)$.

From (46), it is easy to see that it is always possible to select Γ and Y such that the eigenvalues of A can be placed arbitrarily. Assuming that Γ and Y are chosen in such a way that the eigenvalues of A are in the LHP, it is always possible to find a positive definite matrix P such that

$$A^T P + PA = -Q$$

for any given positive definite matrix Q . Let λ_{mQ} denote the smallest eigenvalue of Q . Defining a Lyapunov function as follows:

$$V(e) = e^T P e \quad (48)$$

and evaluating $\dot{V}(e)$ along the trajectories of the system (47)

$$\dot{V}(e) \leq e^T (PA + A^T P) e + 2e^T P B \rho \quad (49)$$

$$\leq -e^T Q e + 2 \|PB\| \|e\| \delta \quad (50)$$

$$\leq -\lambda_{mQ} \|e\|^2 + 2 \|PB\| \|e\| \delta \quad (51)$$

$$\leq \|e\| [\lambda_{mQ} \|e\| + 2 \|PB\| \delta] \quad (52)$$

Therefore, after a sufficiently long time, the norm of the estimation error is bounded by

$$\|e\| \leq \mu \quad (53)$$

Where

$$\mu = \frac{2 \|PB\| \delta}{\lambda_{mQ}} \quad (54)$$

Thus from equation (54), it can be concluded that the norm of the error $\|e\|$ is ultimately bounded and the bounds can be lowered by appropriate choice of control parameters Γ and Y . Thus, the practical stability of the system is proved in the sense of Corless and Leitmann (1981).

3.2 Platform Description and Practical Considerations

LIRMIA III (see Fig. 2) is the AUV developed at the UMI-LAFMIA CINVESTAV Laboratory in Mexico. This vehicle is 60 cm \times 70 cm \times 30 cm in dimension with a weight of 35.8 kg. An acrylic cylinder contains the computer system and electronics. The AUV is equipped with an inertial measurement unit (IMU), a compass for heading, a pressure sensor which is used for depth measurement and two cameras on front and bottom of the vehicle. The propulsion system consists of four thrusters, two heave thrusters, and two yaw thrusters. This configuration implies that the roll motion is not actuated.



Fig. 2. Underwater Vehicle LIRMIA III.

LIRMIA III includes an embedded system which consists of a computer (NUC Intel 4th generation, Core i5-4250U processor, 8GB of DDR3L RAM) that is connected to an external modem through which the submarine's operating system can be accessed remotely. The internal computer runs on the Windows 10 operating system. The system receives data from the AUV sensors, then the data is used by the controller to calculate the torque of the motors and finally, the control signal is sent to the thrusters. The execution time, the data provided by the sensors as well as the torque of the thrusters are monitored by an external computer. The control algorithm was developed using Visual Studio 2012 and runs with a sampling period of $T_s = 180$ ms.

Since the prototype is designed to operate at low speed, it is assumed that the Coriolis matrix does not contribute to vehicle dynamics, i.e., $C(v, \eta) \approx 0$.

In addition, it is considered that M and $D_\eta(v, \eta)$ are diagonal matrices as suggested by Fossen (1994).

In the previous section, the dynamics of an underwater vehicle in its full six degrees of freedom is introduced. In this paper, the proposed controllers will target two degrees of freedom due to the limitations we have in terms of sensors and actuators. For example, in the translational motion, we only can control the depth (z) of the underwater vehicle because the AUV does not have a sensor to measure its position in the plane (x - y). Since in lots of applications we need the vehicle to be close to $\theta = 0$ (pitch) and $\phi = 0$ (roll), which is possible thanks to the design of the vehicle, therefore we have decided to control only the yaw motion (Campos et al. (2017)). Based on the assumptions listed above, the nonlinear model (7) is simplified and following the procedure given at the beginning of the section the control laws shown in (10) and (34) can be rewritten as follows,

$$u_{\psi BS} = I_z [\ddot{\psi}^d + e_1^\psi - \gamma_6 (e_2^\psi + \gamma_6 e_1^\psi) - v_6 e_2^\psi - \frac{N_r}{I_z} \dot{\psi}] \quad (55)$$

$$u_{\psi ST} = I_z [\ddot{\psi}^d - \lambda_6 \dot{e}_1^\psi - k_{16} \phi_1(\phi_2) - k_{26} \int_0^t \phi_2(\sigma_2(\tau)) d\tau] \quad (56)$$

where $u_{\psi BS}$ and $u_{\psi ST}$ are the yaw Backstepping and GSTA controllers. ψ is the yaw measurement provided by the IMU

sensor while $\dot{\psi}$ is the time derivative of yaw. I_z is the inertia moment of the AUV, $e_1^\psi = \psi^d - \psi$, and $\dot{e}_1^\psi = \dot{\psi}^d - \dot{\psi}$ are the yaw error and its time derivative while $e_2^\psi = \dot{\psi} - \dot{\psi}^d - \gamma_6 e_1^\psi$ as defined in corollary 1. Finally, $\phi_1(\sigma_\psi)$ and $\phi_2(\sigma_\psi)$ are the scalar GSTA function given by equations (12) and (13) with $\sigma_\psi = \dot{e}_1^\psi + \lambda_6 e_1^\psi$ and the positive scalar controller gains $\gamma_6, \nu_6, \lambda_6, k_{16}$, and k_{26} .

In turn, the control laws for the immersion test are described as follows:

$$u_{zBS} = m[\ddot{z}^d + e_1^z - \gamma_3(e_2^z + \gamma_3 e_1^z) - \nu_3 e_2^z - \frac{1}{m}(W_B - Z_w \dot{z})] \quad (57)$$

$$u_{zST} = m \left[\ddot{z}^d - \lambda_3 \dot{e}_1^z - k_{13} \phi_1(\sigma_z) - k_{23} \int_0^t \phi_2(\sigma_z) \right] \quad (58)$$

Where u_{zBS} and u_{zST} are the yaw Backstepping and GSTA controllers. Here, m stands for the vehicle mass, while $W_B = (B - mg)$ represents the relationship between vehicle weight and buoyancy (B). $e_1^z = z^d - z$ and $\dot{e}_1^z = \dot{z}^d - \dot{z}$ are the depth error variable and its time derivative while $e_2^z = \dot{z} - \dot{z}^d - \gamma_3 e_1^z$ is the error defined in corollary 1. Finally, $\phi_1(\sigma_z)$ and $\phi_2(\sigma_z)$ are the scalar GSTA functions given by equations (12) and (13) with $\sigma_z = \dot{e}_1^z + \lambda_3 e_1^z$ and the positive scalar controllers gains $\gamma_3, \nu_3, \lambda_3, k_{13}$ and k_{23} .

An important fact to note is that in the sliding mode controller design, the contribution of the matrices $D_\eta(\nu, \eta)$ and $g_\eta(\eta)$ are considered as disturbances, for that reason, the terms of these matrices do not appear in the control laws as in the case of BBSC design.

Remark 4: The simplified control laws (55)-(58) were tested only in the real time experiments, while in simulation test, the control laws given by equations (10) and (34) was applied to the AUV's model of 6 degrees of freedom (for more details of the AUV mathematical model Fossen (1994).

4. SIMULATION RESULTS

To demonstrate the feasibility of the developed controllers (10) and (34), we performed several computer simulation tests with the six degrees of freedom LIRMIA III AUV model. The control parameters are K_1, K_2 and Λ for the GSTA and the set of parameters Γ and Y for the BBSC were obtained under the constraints obtained in proofs of Theorem 1 and Corollary 1 and heuristically tuned (see Table 1).

Table 1. Control gains used for the simulation tests.

Gain	Value
Λ	diag(2,2,2,2,2,2)
K_1	5L
K_2	10L
L	diag(10,10,10,12,12,12)
Γ	diag(7,7,7,10,10,10)
Y	diag(2,2,2,2,2,2)

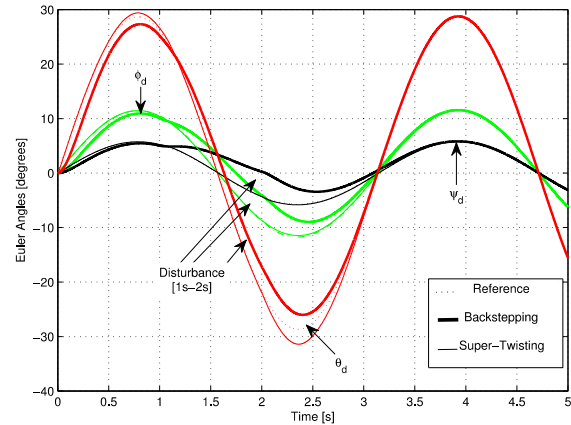


Fig. 3. Tracking a sinusoidal profile for the control of Euler angles θ (red), ϕ (green) and ψ (black).

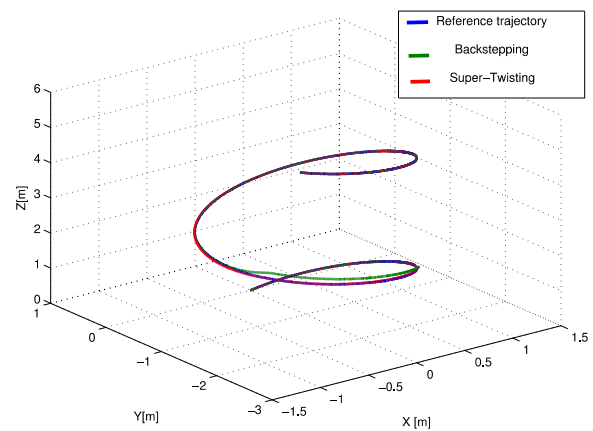


Fig. 4. Comparison between the Super-Twisting (red line) and Backstepping (green line) controller. Trajectory tracking with external disturbance test.

In Fig. 3 the orientation controller performance of the UAV is tested, a sinusoidal profile defined as $[\phi_d(t) = 0.2 \sin(2\pi t), \theta_d(t) = 0.5 \sin(2\pi t), \psi_d(t) = 0.1 \sin(2\pi t)]$ is introduced in those states. In this test, the disturbances vector $u_{pert} = [0, 0, 0, 20, 20, 20]$ introduced at time $t \in [1, 2]$ is considered in the orientation control. From the Fig. 3 it is observed that the GSTA controller has a substantial advantage over the Backstepping methodology when the system is under disturbances.

To test the performance of the position controller, we introduce a three-dimensional spiral function given by the expression:

$$\begin{bmatrix} x \\ y \\ z \end{bmatrix} = \begin{bmatrix} \sin(2t) \\ \cos(2t) - 1 \\ t \end{bmatrix}$$

A constant disturbance is introduced directly on the control at a time $t \in [1, 2]$ of form $u_{pert} = [30, 20, 25, 0, 0, 0]$.

In Fig. 4, it is presented as a comparison between BBSC (green line) and GSTA (red line) controllers for the defined trajectory tracking (blue line). For this simulation, the GSTA

gains remain the same as in the previous case. The BBSC gains are modified as follows $\Gamma = \text{diag}(20, 20, 20, 10, 10, 10)$, while the disturbance is defined as $u_{\text{pert}} = [10, 10, 10, 0, 0, 0]$. Figure 4 shows that the disturbance has a considerable effect on the BBSC despite the fact that the disturbance is numerically smaller than in the case of GSTA controller.

5. REAL-TIME EXPERIMENTAL RESULTS

To demonstrate the practical feasibility of the developed controllers, we applied the controllers described by equations (55), (56), (57) and (58) for yaw and depth tracking trajectories to LIRMIA III. The primary objective of the control laws is to follow a reference trajectory in depth and yaw at the same time despite external disturbances. The reference signal for the yaw control law is $\psi_d(t) = 50\sin(2\pi ft) + 100$ with the frequency $f = \frac{1}{20s}$ and the tracking trajectory for the depth controller is given by the following expressions $z_d(t) = 2 + \frac{1}{2}\sin(2\pi ft)$ with the frequency $f = \frac{1}{20s}$ and the next function:

$$z_d(t) = \begin{cases} (1/15)t & \text{if } t < 60 \\ 4 & \text{if } 60 \leq t < 70 \\ -(3/40)(t-70)+4 & \text{if } 70 \leq t < 90 \\ 2.5 & \text{if } 90 \leq t < 100 \\ -(3/40)(t-100)+2.5 & \text{if } 100 \leq t < 120 \\ 1 & \text{if } 120 \leq t < 130 \\ 1(3/20)(t-150) & \text{if } 130 \leq t < 150 \end{cases} \quad (59)$$

Three types of disturbance test are considered. In the first scenario, the yaw and immersion controllers (independently tested) are disturbed by hand. Second, in the path tracking test an acrylic sheet is installed on the side of the structure of the AUV in order to add damping to the system, especially in the yaw dynamics. Finally, buoyancy is added to the vehicle to introduce a considerable disturbance and modify heave dynamics.

It is important to highlight that in the whole set of experiments, both controllers were tuned heuristically but always considering the constraints given by the stability proofs shown above. The process of tuning the controller gains was divided into two main but simple steps for each methodology. For example, the tuning procedure for the depth Backstepping controller it was the following:

Choosing a constant reference, v_3 is fixed at a value almost zero, and α_3 is increased until the closed loop system oscillates.

Then, the gain α_3 is decreased respect of its last value, and the gain v_3 is increased until reach the desired constant value without controller oscillations.

For the tuning of the depth controller using GSTA, it could be seen as a nonlinear PI controller, where we can follow the same methodology used for the BBSC, the procedure is enclosed as follows:

We fix the values $\lambda_3 = 1$ and $k_{23} = 0.0001$ and the gain k_{13} is increased until the controller reaches the desired value and starts to oscillate.

Decrease a fraction of k_{13} and then increase the value of k_{23} slightly until the oscillation in steady state decrease.

Due to the large sample period and in order to prevent the chattering effect in the control signal of the GSTA, it is suggested to keep the gain k_{23} in a small value. After tuning the controllers for a constant reference, the control laws were tested for a trajectory tracking task without considering external disturbances, where the values of the gains were improved until reach a good performance and can be seen in Table 2. Finally, the gains found with the previous procedure were unchanged during the robustness tests.

Table 2. Control gains used for the experiments.

Gain	Value
γ_3	5.0
v_3	4.0
λ_3	1.0
k_{13}	2.0
k_{23}	0.01
γ_6	8.0
v_6	4.0
λ_6	1.0
k_{16}	0.9
k_{26}	0.02

5.1 Path tracking test on uncoupled dynamics

In this stage, the yaw and depth controllers were independently tested and externally disturbed. In Figure 5, the tracking of a sinusoidal signal for yaw displacements is shown. Both control laws, BBSC and GSTA, can follow the reference signal after a relatively short adaptation time. It is clear that experiments started from different initial conditions due to experimental restrictions. It is worth mentioning that GSTA control law has shown better performance at least in two aspects, the error (figure not shown here for space reasons) is of lower magnitude, and second, it can compensate external disturbances faster than BBSC control and with a lower overshoot, see Fig. 5.

In turn, in Figure 6, controller performances when dealing with a sinusoidal profile tracking of depth are shown. In this case, the convergence to the reference signal is almost identical for GSTA and BBSC. After external disturbances, both controllers return to the commanded signal, however, the BBSC controller has an offset in its signal.

In order to evaluate the trajectory tracking performance of the GSTA and BBSC methodologies, it is computed the Root Mean Square Error (RMSE) for z and ψ motions which are summarized in Table 3. From the Table 3, it is possible to observe that the GSTA controller has better numerical results than the Backstepping controller.

Table 3. Root Mean Square Error performance for sinusoidal function tracking test.

Controller	RMSE $_{\psi}$ (deg)	RMSE $_z$ (m)
Backstepping	6.2846	0.7890
Sliding Modes	2.9294	0.6479

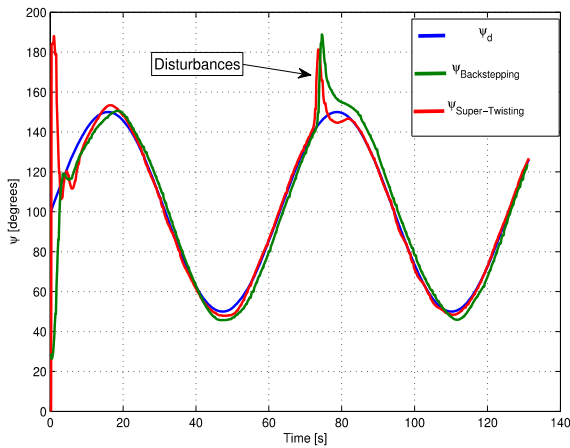


Fig. 5. Yaw angle reference tracking test. Super-Twisting (red) and Backstepping (green) controllers performance.

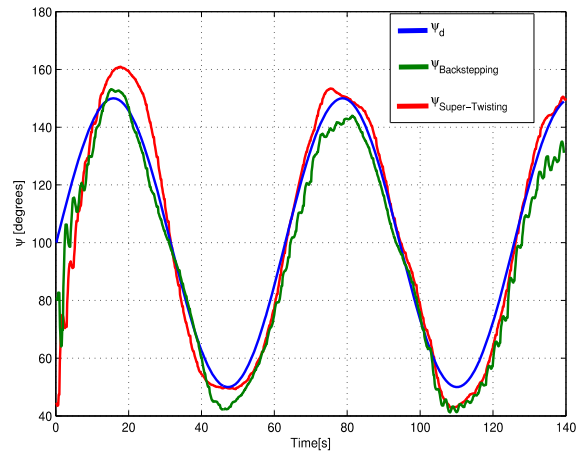


Fig. 7. Path tracking with yaw damping test. Super-Twisting (red) and Backstepping (green) controllers following reference (blue).

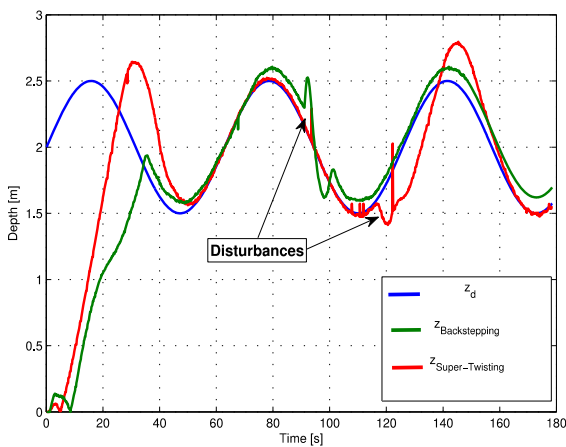


Fig. 6. Tracking immersion test. Super-Twisting (red) and Backstepping (green) controllers performance.

5.2 Tracking in presence of disturbance damping

A more challenging test consisted of installing a large (74.5cm x 20 cm) rigid acrylic sheet on one side of the AUV to add damping to the system (yaw motion), this plate is proportional to the length of the submarine and increases the rotational damping along the z axis of about 125%. Yaw and depth controllers follow a reference signal at the same time.

In Figures 7 and 8 the performance of the proposed controller is observed. From Fig. 7, damping effect added by the side sheet is observed, but even with this disturbance, both controllers can follow the sinusoidal trajectory. Moreover, Fig. 8 shows the profile tracking where the GSTA has an exact convergence. Otherwise, the spiral formed by the two movements together is shown in Fig. 9. The RMSE for yaw and depth during the test with damping test is shown in Table 4.

Finally, Figures 10 and 11 show the tracking errors and the corresponding controllers outputs.

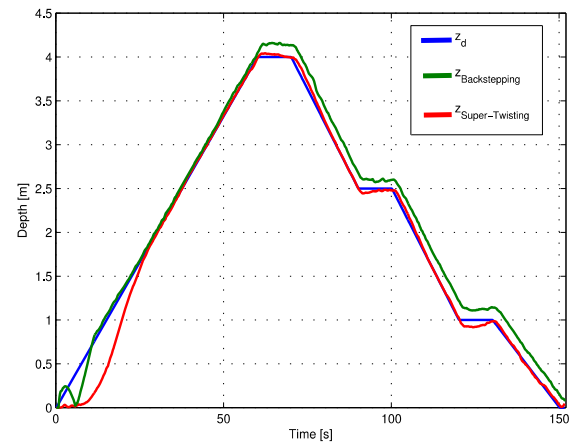


Fig. 8. Immersion test adding damping to Yaw. Super-Twisting (red) and Backstepping (green) controllers performance.

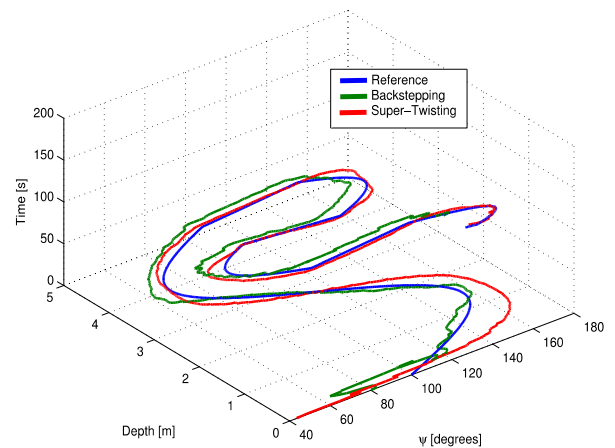


Fig. 9. Trajectory tracking with combined movements in ψ and z .

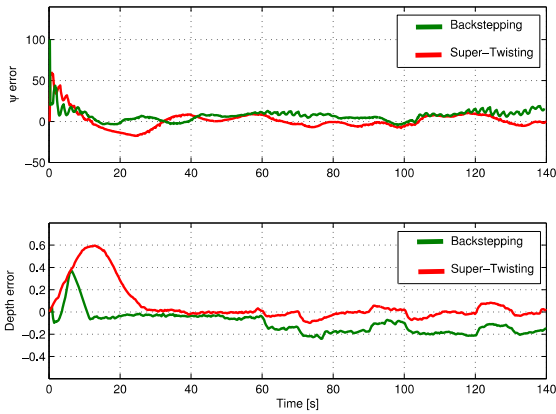


Fig. 10. Tracking error in damping test. Super-Twisting (red) and Backstepping (green) errors.

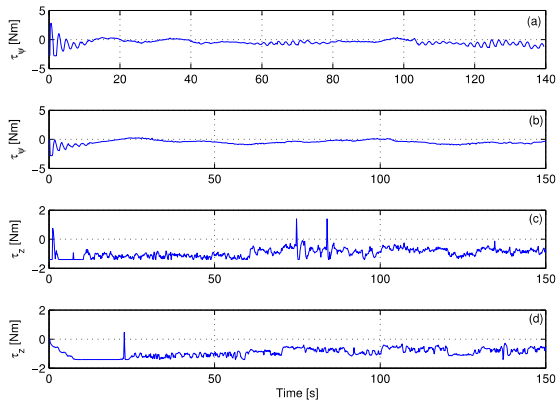


Fig. 11. Controller outputs in damping test. (a) yaw BBSC, (b) yaw GSTA, (c) depth with BBSC and (d) depth with GSTA.

Table 4. Root Mean Square Error for tracking test with a disturbance in damping parameters.

Controller	RMSE $_{\psi}$ (deg)	RMSE $_z$ (m)
Backstepping	8.1504	0.1442
Sliding Modes	9.7041	0.0548

5.2 Tracking in presence of disturbance buoyancy

In contrast to the previous test, buoyancy is added to the vehicle greatly hindering immersion test. In this scenario, three floating balls with 8 cm of diameter were attached to the vehicle which increases the buoyancy around of 200%. Fig. 12 shows the tracking controller performance, BBSC presents oscillations while GSTA converges in a short time. In Fig. 13, the BBSC has superior performance to GSTA in the trajectory tracking, this is reasonable since the GSTA controller, the terms of buoyancy in the model are not considered and therefore not compensated appropriately in the proposed control law. The RMSE behavior for the trajectory tracking test with buoyancy disturbance is shown in Table 5. From the Table 5, it can be observed that GSTA has better performance than BBSC, but this methodology has lower tracking error than GSTA controller.

Finally, Figures 14 and 15 show the tracking errors and the corresponding controllers outputs. One may notice that control efforts are similar in the previously cases with both

GSTA and BBSC control laws. Nevertheless, the control effort is much more demanding in the case of BBSC control law when considering depth regulation or depth tracking. Remark that no undesirable chattering effects due to GSTA control technique are observed.

Table 5. Root Mean Square Error for tracking test with a disturbance in buoyancy parameters.

Controller	RMSE $_{\psi}$ (deg)	RMSE $_z$ (m)
Backstepping	9.2645	0.2263
Sliding Modes	6.6338	0.5744

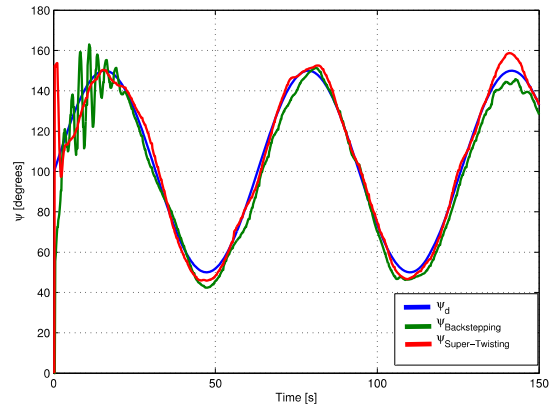


Fig. 12. Path tracking with buoyancy test. Super-Twisting (red) and Backstepping (green) controllers following reference (blue).

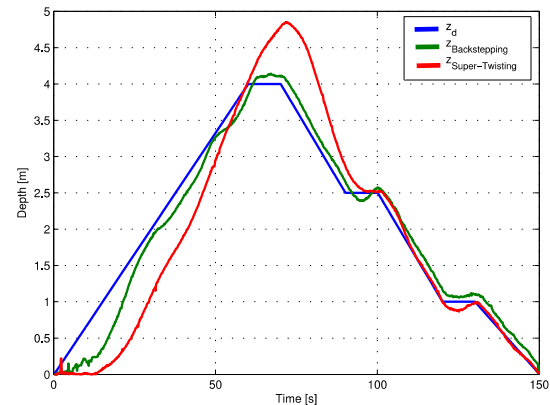


Fig. 13. Immersion with buoyancy test. Super-Twisting (red) and Backstepping (green) controllers performance.

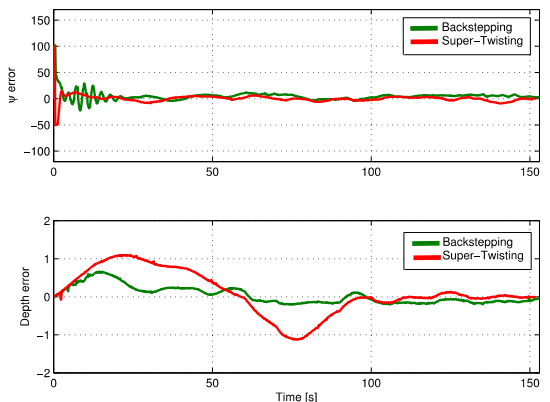


Fig. 14. Tracking error in buoyancy test. Super-Twisting (red) and Backstepping (green) errors.

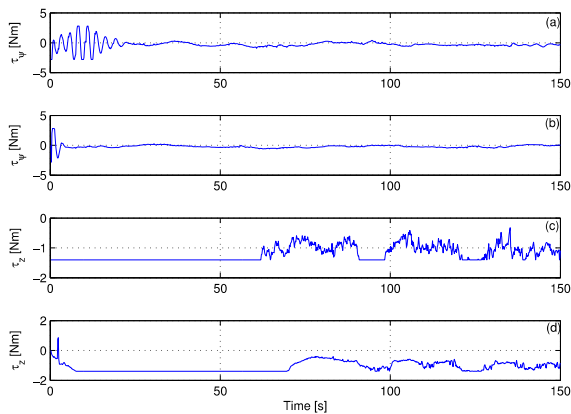


Fig. 15. Controller outputs in buoyancy test. (a) yaw BBSC, (b) yaw GSTA, (c) depth with BBSC and (d) depth with GSTA.

6. CONCLUSIONS AND FINAL REMARKS

6.1 Conclusions

This article describes two controllers that were presented to solve the problem of trajectory tracking for an autonomous underwater vehicle under model uncertainties and external disturbances. For the controller description, the nonlinear model of UAV is used. Nonlinear control techniques used were Block-Backstepping and Higher-Order Sliding Modes with Generalized Super-Twisting Algorithm. As a matter of comparison, real-time control experiments have shown better performances when considering the Sliding Modes Control paradigm.

6.1 Ongoing work

In this work, the tracking problem of trajectories involving coordinated displacements on both yaw and depth were considered. Trajectory tracking in pitch and displacements in Y are a subject of our future research work. The theoretical and real-time results given in this paper are promising to deal with more complex trajectory tracking problems where Sliding Mode Control might take a prominent place.

ACKNOWLEDGMENTS

This work was supported by Conacyt (Mexico), grant 490978. The authors gratefully thank to the Referee for the constructive comments and recommendations which definitely help to improve the readability and quality of the manuscript.

REFERENCES

Aguiar, A.P. and Hespanha, J.P. (2007). Trajectory-tracking and path-following of underactuated autonomous vehicles with parametric modeling uncertainty. *IEEE Transactions on Automatic Control*, 52(8), 1362–1379.

Akakaya, H., Yildiz, H.A., Salam, G., and Grleyen, F. (2009). Sliding mode control of autonomous underwater vehicle. In Electrical and Electronics Engineering, 2009. ELECO 2009. *International Conference on*, II–332–II–336.

Campos, E., Chemori, A., Creuze, V., Torres, J., and Lozano R. (2017). Saturation based nonlinear depth and yaw

control of underwater vehicles with stability analysis and real-time experiments. In *Mechatronics*, 45, 49–59.

Campos, E., Monroy, J., Abundis, H., Chemori, A., Creuze, V., and Torres, J. (2018). A nonlinear controller base don saturation functions with variable parameters to stabilize an AUV. *International Journal of Naval Architecture and Ocean Engineering*.

Corless, M. and Leitmann, G. (1981). Continuous state feedback guaranteeing uniform ultimate boundedness for uncertain dynamic systems. *IEEE Transactions on Automatic Control*, 26(5), 1139–1144.

Encarnacao, P. and Pascoal, A. (2001). Combined trajectory tracking and path following: an application to the coordinated control of autonomous marine craft. In *Decision and Control*, 2001. *Proceedings of the 40th IEEE Conference on*, volume 1, 964–969. IEEE.

Fossen, T.I. (1994). Guidance and control of ocean vehicles. *John Wiley & Sons Inc*.

Fossen, T.I. (2002). Marine control systems: guidance, navigation and control of ships, rigs and underwater vehicles.

Hoang, N.Q. and Kreuzer, E. (2007). Adaptive pd controller for positioning of a remotely operated vehicle close to an underwater structure: theory and experiments. *Control Engineering Practice*, 15(4), 411–419.

Ismail, Z.H. and Putranti, V.W. (2015). Second order sliding mode control scheme for an autonomous underwater vehicle with dynamic region concept. *Mathematical Problems in Engineering*, 2015.

Kawano, H. and Ura, T. (2002). Fast reinforcement learning algorithm for motion planning of nonholonomic autonomous underwater vehicle in disturbance. In *Intelligent Robots and Systems, 2002. IEEE/RSJ International Conference on*, volume 1, 903–908 vol.1. doi:10.1109/IRDS.2002.1041505.

Kinsey, J.C., Eustice, R.M., and Whitcomb, L.L. (2006). A survey of underwater vehicle navigation: Recent advances and new challenges. In *IFAC Conference of Manoeuvring and Control of Marine Craft*, volume 88.

Lapierre, L., Soetanto, D., and Pascoal, A. (2003). Non-linear path following with applications to the control of autonomous underwater vehicles. In *Decision and Control, 2003. Proceedings. 42nd IEEE Conference on*, volume 2, 1256–1261. IEEE.

Li, Y., Jiang, Y.q., Wang, L.f., Cao, J., and Zhang, G.c. (2015a). Intelligent pid guidance control for auv path tracking. *Journal of Central South University*, 22, 3440–3449.

Li, Y., Wei, C., Wu, Q., Chen, P., Jiang, Y., and Li, Y. (2015b). Study of 3 dimension trajectory tracking of underactuated autonomous underwater vehicle. *Ocean Engineering*, 105, 270–274.

Liang, X., Wan, L., Blake, J.I., Shenoi, R.A., and Townsend, N. (2016). Path following of an underactuated auv based on fuzzy backstepping sliding mode control. *International Journal of Advanced Robotic Systems*, 13(3), 122.

Moreno, J.A. (2009). A linear framework for the robust stability analysis of a generalized super-twisting algorithm. In *Electrical Engineering, Computing Science*

- and Automatic Control*, CCE, 2009 6th International Conference on, 1–6. IEEE.
- Perrier, M. and Canudas-De-Wit, C. (1996). Experimental comparison of pid vs. pid plus nonlinear controller for subsea robots. *Autonomous Robots*, 3(2), 195–212. doi:10.1007/BF00141155. URL <http://dx.doi.org/10.1007/BF00141155>.
- Prestero, T.T.J. (2001). Verification of a six-degree of freedom simulation model for the REMUS autonomous underwater vehicle. Ph.D. thesis, *Massachusetts institute of technology*.
- Sahu, B.K. and Subudhi, B. (2014). Adaptive tracking control of an autonomous underwater vehicle. *International Journal of Automation and Computing*, 11(3), 299–307.
- Salgado-Jiménez, T., García-Valdovinos, L.G., and Delgado-Ramírez, G. (2011). Control of rovs using a model-free 2nd-order sliding mode approach. In *Sliding mode control*, 347–368. InTech.
- Shtessel, Y., Edwards, C., Fridman, L., and Levant, A. (2014). Sliding mode control and observation. *Springer*.
- Sun, B., Zhu, D., and Yang, S.X. (2014). A bioinspired filtered backstepping tracking control of 7000-m manned submarine vehicle. *IEEE Transactions on Industrial Electronics*, 61(7), 3682–3693.
- Szymak(2016). Using neuro-evolutionary-fuzzy method to control a swarm mode control of autonomous of unmanned underwater vehicles. In *Journal of Control Engineering and Applied Informatics*, 18(3), 82-92. 9. International Conference on, II–332–II–336.
- Wadoo, S.A., Sapkota, S., and Chagachagere, K. (2012). Optimal control of an autonomous underwater vehicle. In *Systems, Applications and Technology Conference (LISAT)*, 2012 IEEE Long Island, 1–6. doi: 10.1109/LISAT.2012.6223100.
- Wang, Y., Yan, W., Gao, B., and Cui, R. (2009). Backstepping-based path following control of an underactuated autonomous underwater vehicle. In *Information and Automation, 2009. ICIA'09. International Conference on*, 466–471. doi: 10.1109/ICINFA.2009.5204969.
- Wu, H.M. and Karkoub, M. (2014). Hierarchical backstepping control for trajectory-tracking of autonomous underwater vehicles subject to uncertainties. In *Control, Automation and Systems (ICCAS)*, 2014 14th International Conference on, 1191–1196. IEEE.
- Xiang, X., Lapiere, L., Liu, C., and Jouvencel, B. (2011). Path tracking: combined path following and trajectory tracking for autonomous underwater vehicles. In *2011 IEEE/RSJ International Conference on Intelligent Robots and Systems*, 3558-3563. IEEE.